

Integrated Simulation Modeling Approach for Investigating Pore Water Pressure Induced Landslides

Sahila Beegum (✉ beegumsahila@gmail.com)

University of Nebraska-Lincoln <https://orcid.org/0000-0003-3623-4426>

P J Jainet

Kerala State Council for Science Technology and Environment

Dawn Emil

Kerala State Council for Science Technology and Environment

K P Sudheer

Kerala State Council for Science Technology and Environment

Saurav Das

University of Nebraska-Lincoln

Research Article

Keywords: Landslide, Factor of safety, HYDRUS-2D/3D, GeoStudio-Slope/W, Pressure head, Pore water pressure, Extreme rainfall events

Posted Date: January 13th, 2022

DOI: <https://doi.org/10.21203/rs.3.rs-1186263/v1>

License:  This work is licensed under a Creative Commons Attribution 4.0 International License.

[Read Full License](#)

23 stability of hillslope, and simulation results were found to be co-aligned with the actual landslide that
24 occurred in 2018. Simulations were carried out for natural and modified hill slope geometry in the study
25 area. The volume of water in the hill slope, temporal and spatial evolution of pore water pressure, and
26 factor of safety were analysed. Results indicated higher stability in natural hillslope (factor of safety of
27 1.243) compared to modified hill slope (factor of safety of 0.946) despite a higher pore water pressure
28 in the natural hillslope. The study demonstrates the integrated applicability of the physics-based models
29 in analyzing the stability of hill slopes under varying pore water pressure and hill slope geometry and its
30 accuracy in predicting future landslides.

31 **Keywords:** Landslide, Factor of safety, HYDRUS-2D/3D, GeoStudio-Slope/W, Pressure head,
32 Pore water pressure, Extreme rainfall events

33 **Highlights:**

- 34 - Demonstration of the integrated application of physics-based models in analyzing the stability of
35 hill slopes under varying pore water pressure and hill slope geometry
- 36 - Correlation of evolution of pore water pressure, factor of safety, and geometry of hill slope to
37 the landslide occurrence

38

39 **1. Introduction**

40 According to World Health Organization (WHO), landslides affected 4.8 million people and caused
41 more than 18,000 deaths in the world between 1988 - 2017 (WHO, 2018). Prolonged and heavy rainfalls
42 are the major factors causing landslides (Petley, 2012). In the past several years, the frequency of
43 rainfall-induced landslides has increased with extreme rainfall events and anthropogenic activities (Marc
44 et al., 2018; Rahimi et al., 2010). Climate change and frequent flash floods have also aggravated the
45 landslide issues. Slope stability analysis can help understand the causes and potential triggers for a slope
46 failure and aid in its mitigation. In the case of stability analysis of rainfall-induced landslides, it is

47 essential to correlate the rainfall threshold and pore water pressure (PWP) threshold with the factor of
48 safety by considering the changes in the physical and hydraulic properties of the soil. An accurate
49 prediction of pore water pressure is fundamental for assessing slope stability in saturated soils. Though
50 the landslide occurs within minutes, the soil moisture condition building up that ultimately triggers the
51 landslides may take several hours to days. During a rainfall event, the pore water pressure varies
52 temporally and spatially based on the (a) intensity and duration of the rainfall, (b) geometry of the soil
53 layers and hillslope, (c) soil hydraulic properties and index properties, and (d) land use and land cover
54 (Huang et al., 2012; Rahardjo et al., 2008b). Variations in the pore water pressure will impact the matric
55 suction, effective stress, and soil stability (Rahardjo et al., 2008b). It is essential to account for these
56 variabilities through accurate physical representation while investigating the slope stability. These
57 parameters are crucial for understanding the initiation of landslide processes in a location and future
58 landslide prediction for the mitigation approach (Carey et al., 2019; Kim et al., 2017; Liang, 2020).

59 There are several limitations in analyzing the real-time pore water pressure evolution in field-scale/
60 laboratory-scale studies during the occurrence of a landslide. In most cases, the piezometers and other
61 instruments installed to monitor real-time pore water pressure and landslide displacement gets damaged
62 during landslides with large displacements (Matsuura et al., 2008). Besides, pore water pressure
63 determination becomes more complex when the hill slope has highly heterogeneous soil layers, leading
64 to complex flow dynamics in the unsaturated-saturated soil zone. Since the pore water pressure
65 distribution rarely follows a linear distribution along the depth or a uniform response across the slope,
66 accurate measurement of pore pressure would require a large number of sensors. The measurements
67 become more complex in the presence of subsurface conduits (soil pipes, burrows, etc.) (Fannin &
68 Jaakkola, 1999; Hopkins et al., 1975; Johnson & Sitar, 1990). Due to these limitations, transient nature
69 pore water pressure is mainly studied as an approximation of the actual response (Kuriakose et al., 2008;
70 Oh & Lu, 2015). A better alternative is to utilize integrated simulation models that simulate water flow
71 through the unsaturated-saturated soil zones and carry out slope stability analysis by considering the

72 change in pore water pressure due to the water flow dynamics. Simulation models can also assist in
73 analyzing the spatio-temporal variation in the evolution of pore water pressure with the change in the
74 hill slope geometry (due to natural or anthropogenic activities).

75 GeoStudio-Slope/W (Geo-Slope, 2012) is a widely used simulation model for slope stability analysis
76 (Jalilzadeh et al., 2020; Bui et al., 2020; Mishal & Khayyun, 2018). It can simulate a variety of slip
77 surface shapes, pore water pressure conditions, analysis methods, and loading conditions. Pore water
78 pressures accounted in the stability analysis in GeoStudio-Slope/W can be defined using piezometric
79 lines or spatial functions or from GeoStudio finite element analysis model (Seep/W). Since pore water
80 greatly influences the stability of the slope, GeoStudio-Slope/W model should be provided with accurate
81 pore water pressure information (D. Fredlund, 1987; Rahardjo et al., 2008a; Xu & Yang, 2018). Among
82 various simulation models for water flow dynamics and pore water pressure estimation in unsaturated-
83 saturated soil zones, HYDRUS-2D/3D has been extensively used to predict pore water pressure
84 dynamics (Karandish & Šimůnek, 2019; Lehmann et al., 2013). An approach towards improving slope
85 stability analysis using GeoStudio-Slope/W can be achieved by integrating the pore water pressure
86 measurements from HYDRUS-2D/3D into GeoStudio-Slope/W. Jalilzadeh et al., 2020 studied that
87 HYDRUS-1D has more database on soil/vegetation functions and offers less computational time than
88 GeoStudio-Seep/W (commonly used finite element model for pore water estimation in GeoStudio-
89 Slope/W). HYDRUS-2D/3D can consider root water uptake, hysteresis, and tortuosity in the soil.
90 HYDRUS-based simulations programs are already integrated with other models like MODFLOW
91 (Beegum et al., 2018, 2019), AQUACROP (Kanda et al., 2021), etc., due to its modeling capabilities
92 compared to other existing models.

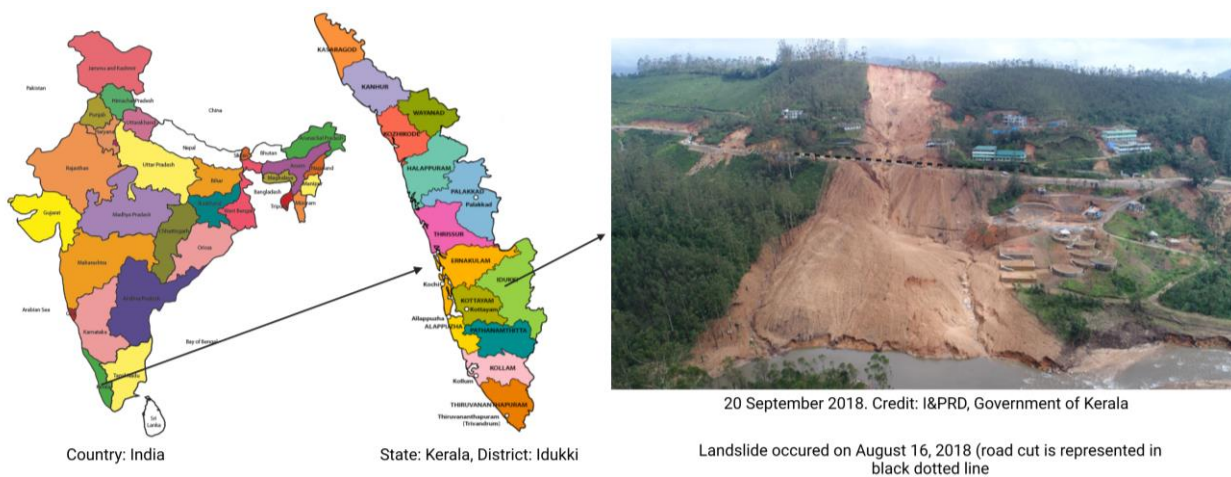
93 The objective of the study was to analyze the evolution of PWP and its relation to the hillslope stability
94 using the integrated application of simulation models (HYDRUS-2D/3D and GeoStudio-Slope/W). As
95 a case study, a hill slope in Kerala, India, that has undergone a modification in the natural hillslope was

96 considered. Kerala Planning Board (KPB), 2019 reported 143 major landslides in this district, which
97 was the highest recorded in the country in 2018. This study dictates the integrated application of the
98 simulation models as a tool to understand and predict the landslide process. This study will help identify
99 and predict future landslide-prone areas and design a subsequent mitigation approach to save human and
100 property damages or warning before the incidence.

101 2. Materials and Methods

102 2.1. Study design

103 The study area considered was a hillslope in Munnar (10.087°N Latitude, 77.094°E Longitude) in the
104 district of Idukki in Kerala, India. A massive slide occurred at this location on 16th August 2018 (Fig.
105 1).



106
107 Fig. 1. The country India, Kerala state, Idukki district, and a photograph of the landslide occurred on
108 16th August 2018.

109 Specific objectives of the study were to analyze; (a) PWP evolution corresponding to the extreme rainfall
110 event that occurred in August 2018 (which was the month with the highest recorded rainfall in the year)
111 and (b) the impact of modification of the natural hill slope on slope stability. Two different cases were
112 analyzed: Case 1: a case with road cut in the hill slope (hill slope after slope modification), and Case 2:

113 a case without road cut in the hill slope (natural hillslope). Case 1 corresponds to the prevailing slope in
114 this area before the landslide occurred in 2018. Case 2 is an assumption made to analyze the potential
115 impact of the extreme rainfall event if natural hillslope existed in this area (Fig. 2).

116 2.2. Simulation models and modeling approach

117 2.2.1. HYDRUS-2D/3D

118 HYDRUS-2D/3D (Šimůnek et al., 2016) is a physics-based model for simulating water, heat, and solute
119 movement in two- and three-dimensional variably saturated media. The advantages of HYDRUS-2D/3D
120 lie in its ability to simulate highly heterogeneous soil layers, variable boundary conditions, the automated
121 time-stepping algorithm for simulation optimization, etc. Several studies have demonstrated the
122 capabilities of HYDRUS-2D/3D in simulating the pressure head/PWP and moisture content variation in
123 the unsaturated and saturated soil zones (Beegum et al., 2018, 2019; Simunek et al., 2018; Šimůnek et
124 al., 2016). The modeling of water flow and transfer and transformation of the solute consider soil
125 hydraulic properties, solute transport parameters, environmental factors (precipitation, evaporation rate,
126 transpiration rate), plant water uptake, and various boundary conditions. The HYDRUS-2D/3D model
127 solves water flow in the unsaturated zone using the modified two-dimensional Richards' equation:

128

$$129 \quad \frac{\partial \theta(h)}{\partial t} = \frac{\partial}{\partial x_i} \left[K(h) \left(K_{ij}^A \frac{\partial h}{\partial z} + K_{iz}^A \right) \right] - S(h)$$

130

131 where θ is the volumetric water content (dimensionless), h is the soil water pressure head [L], t is time
132 [T], z is the vertical coordinate [L], S is the sink term [T^{-1}], and $K(h)$ is the unsaturated hydraulic
133 conductivity [LT^{-1}]. K_{ij}^A is the components of dimensionless anisotropy tensor K^A , $S(h)$ is the sink/
134 source term [$L^3L^{-3}T^{-1}$] and x_i is the spatial coordinate [L]. The unsaturated hydraulic conductivity, $K(h)$,
135 and water content, θ , depends on the soil water pressure head (h). This makes Richards' equation a
136 highly nonlinear equation that needs to be solved numerically. HYDRUS-2D/3D permits using five

137 different analytical models to describe the soil hydraulic properties (Brooks & Corey, 1964; Durner,
138 1994; Kosugi, 1996; Van Genuchten, 1980; Vogel & Cislerova, 1988).

139 **2.2.2. GeoStudio-Slope/W model**

140 GeoStudio-Slope/W model is developed based on the general limit equilibrium (GLE) formulation
141 (Fredlund & Krahn, 1977). This formulation is based on two factors of safety equations; (a) the factor
142 of safety with respect to moment equilibrium and (b) the factor of safety with respect to horizontal force
143 equilibrium (Spencer, 1967). The interslice shear forces in the GLE formulation are based on the
144 equation proposed by Morgenstern and Price (Morgenstern & Price, 1965):

$$145 \quad X = E\lambda f(x)$$

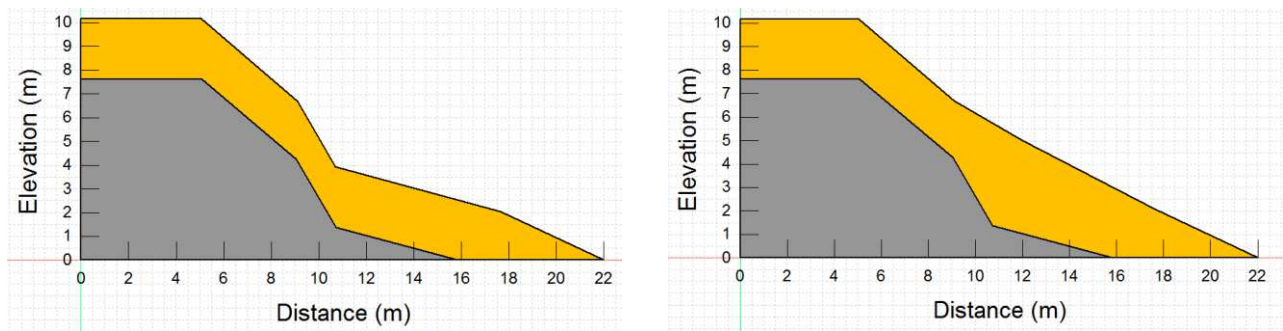
146 Where $f(x)$ is the function describing the distribution of internal forces, λ is the percentage of the function
147 used, E is the interslice normal force, and X is the interslice shear force.

148 **2.2.3. Integration of HYDRUS-2D/3D with GeoStudio-Slope/W model**

149 The integrated application of two different models was performed to utilize the advantages of HYDRUS-
150 2D/3D in its accurate estimation of the pore water pressure with the stability analysis capabilities of the
151 GeoStudio-Slope/W module. HYDRUS-2D/3D solves the water flow in the soil using a finite element
152 formulation. A finite element mesh was generated in the soil domain of the hillslope by dividing the
153 flow region into quadrilateral or triangular elements (Fig. 5). Once the water flow simulations were
154 carried out using HYDRUS-2D/3D, the pore water pressure at the nodes that form the corners of the
155 elements was extracted for discrete time intervals. The time variable pore water pressure distribution
156 was mapped into the GeoStudio-Slope/W model corresponding to the discrete-time intervals and spatial
157 locations. The slope stability analysis in the GeoStudio-Slope/W model was then carried out based on
158 these pore pressure distributions.

159 **2.3. Model setup**

160 The input data required for simulations using HYDRUS-2D/3D and GeoStudio-Slope/W were (a) cross-
 161 sectional details of the hill slope, (b) soil physical and hydraulic properties, and (c) initial and boundary
 162 conditions. The cross-sectional details of the hill slope and soil properties in the study area were obtained
 163 based on the field investigation to examine the causes of repeated extreme heavy rainfall events,
 164 subsequent floods, and landslides in Kerala (Kerala Planning Board, 2019; Choudhury et al., 2019). The
 165 geometry of the hill slope in Case1 (with road cut) and Case 2 (without road cut) is shown in Fig. 2. The
 166 average angle of elevation is 24.8° . The maximum depth of the soil (shown in yellow color in Fig. 2)
 167 above the rock (shown in grey color in Fig. 2) in Case 1 is 2.3 m, and for Case 2 is 4.4 m.



Case 1: With road cut

Case 2: Without road cut

168 Fig. 2. The geometry of the hill slope in Case1 and Case 2. The yellow-colored region represents the
 169 soil layer, and the grey-colored area represents the rock.

170 Table 1. Index and engineering properties of the soil in the hill slope

Moisture content (%)	Bulk density (g/cc)	Shear strength parameters		Grain size distribution (%)			Consistency limits (%)	
		c (kPa)	ϕ (degree)	Silt+clay	Sand	Gravel	Liquid limits	Plastic limits
4.26-18.8	1.34-1.76	2.0-74.0	22.29-36.69	20-76	21-54	1.0-40	34.5-63.1	22.9-35.31

171
 172 Table 1 shows the index and engineering properties of the soil in the hill slope. The unit weight of the
 173 rock was considered as 29.4 KN/m^3 . This corresponds to the rock type - Peninsular Gneissic Complex

174 (PGC) observed in the north region Idukki district represented by granite gneiss (District Survey Report
175 of Minor Minerals, Idukki District, Department of Mining and Geology, 2016). The van Genuchten-
176 Mualem analytical model (van Genuchten, 1980) was used to describe the hillslope soil hydraulic
177 properties with the parameters given in table 2.

178 Table 2. van Genuchten-Mualem analytical model parameters

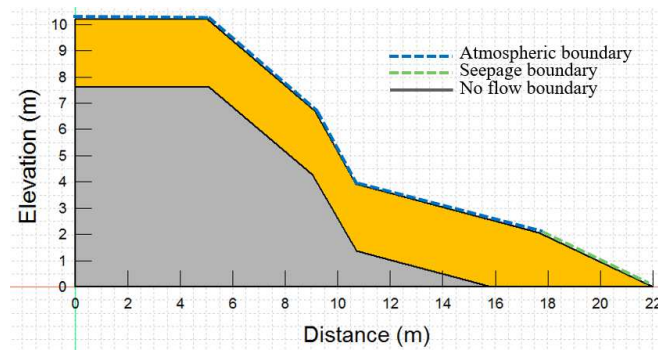
van Genuchten-Mualem analytical model parameters	Values
Residual water content, θ_r	0.077
Saturated water content, θ_s	0.425
Saturated hydraulic conductivity, K_s	1.5 m day ⁻¹
Pore connectivity parameter, l	0.5
Shape parameters, α and n	$\alpha = 1.37 \text{ m}^{-1}$, $n = 1.4027$

179

180 These parameters were obtained using the neural network prediction of soil hydraulic properties using
181 the Rosetta Lite V.1.1 (Schaap et al., 2001). The specific weight of water was considered as 10 KN/m³.

182 2.3.1. Initial and boundary condition

183 In both cases (Case 1 and Case 2), a hydrostatic pressure head distribution was considered in the soil
184 domain at the beginning of the simulation. The left boundary and the bottom of the soil layer (or the top
185 of the rock layer) were considered to have a no-flow boundary. A seepage boundary was given at the
186 extreme right slope of the domain for a depth of 2 m (Fig. 3). In the seepage boundary, when the node
187 next to seepage face becomes saturated, water is immediately removed by overland flow, which in
188 HYDRUS-2D/3D is considered to be removed from the system.



189

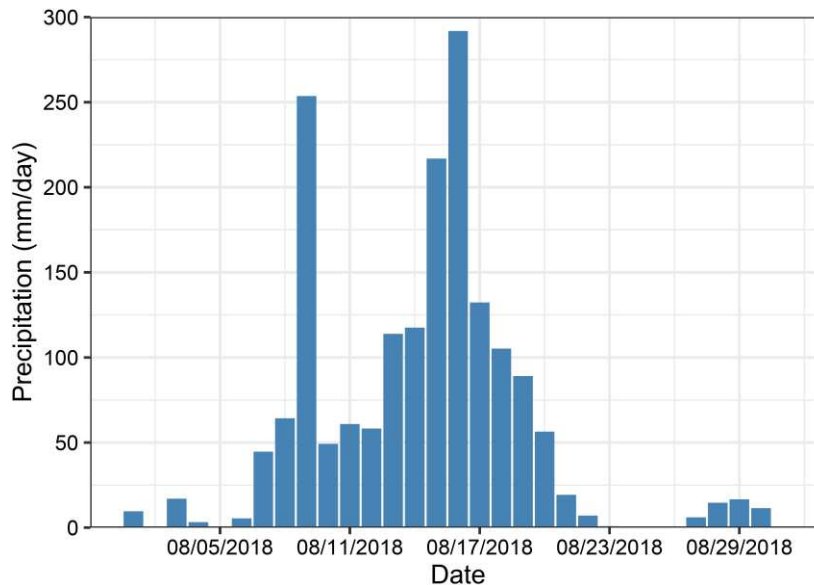
190 Fig. 3. Boundary conditions (atmospheric boundary, seepage boundary and no-flow boundary)

191

considered in the study.

192 **2.3.2. Surface boundary condition**

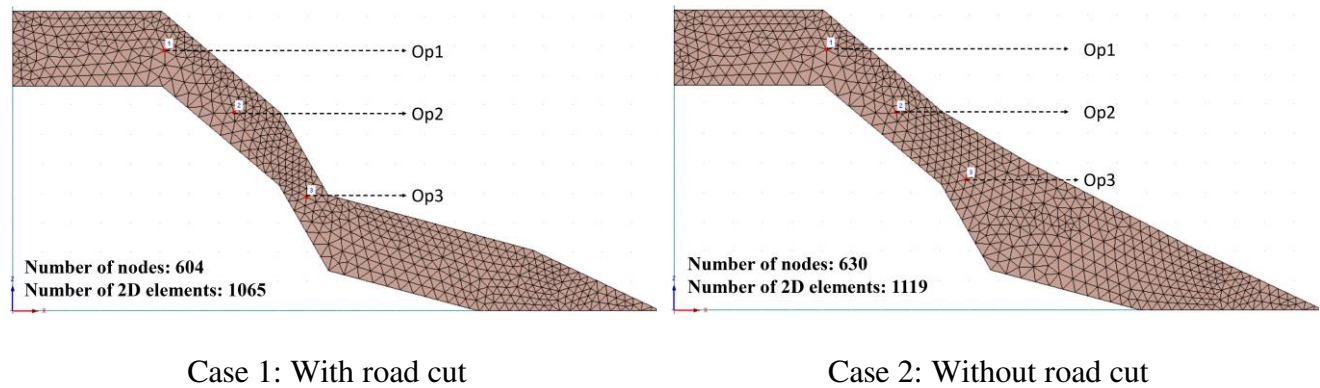
193 To simulate the landslide event in August 2018 in Munnar, the daily rainfall data for this month was
 194 used as the atmospheric boundary condition on the slope surface. This data was obtained from the Indian
 195 Meteorological Department (IMD) for the weather station in Munnar. The maximum rainfall in August
 196 2018 recorded in this station was 291.8 mm/day on 16th August 2018, followed by 253.6 mm/day on 9th
 197 August 2018. Transpiration from the surface of the soil was not considered in the analysis. Figure 4
 198 shows the rainfall for August 2018 in Munnar.



199

200 Fig. 4. Precipitation in mm/day in August 2018 in Munnar IMD station

201 The simulation was carried out for 31 days, corresponding to the number of days in August 2018. The
202 model was simulated to analyze the pore water pressure on each day. A finite element unstructured
203 triangular mesh was developed in the model with a finer resolution at the soil surface. Three observation
204 points (Op1, Op2, and Op3) were specified in the soil domain (Fig. 5).



205 Fig. 5. The unstructured triangular mesh, observation points (Op1, Op2, Op3), and the number of finite
206 elements and nodes considered in the study.

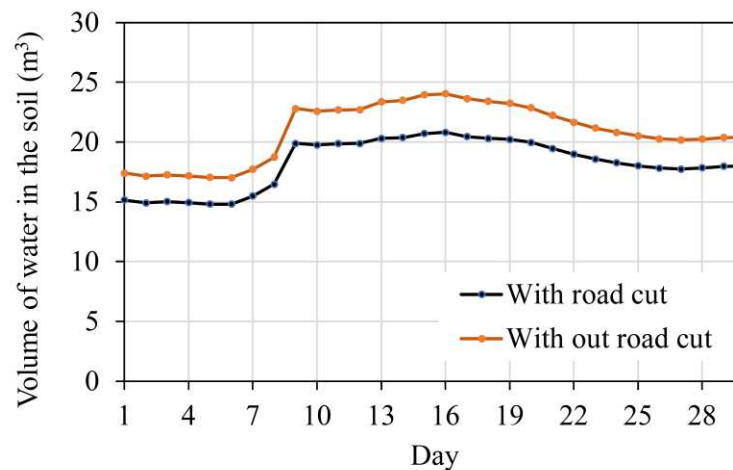
207 3. Results and Discussion

208 Model simulations for Case 1 and 2 were carried out based on the integration methodology discussed in
209 section 2.2.3. The variation in the volume of the water in the hill slope domain, variation in the moisture
210 content at different observation points, pore water pressure distribution, and the factor of safety were
211 analyzed in the hill slope corresponding to the rainfall event in August 2018 and are discussed in the
212 following sections.

213 3.1. Variation in the volume of water in the domain

214 The analysis of total volume of the water in the hillslope soil is important because of its correlation with
215 landslide activity. Klose et al., 2012; Wicki et al., 2020 used soil moisture characteristics for determining
216 the water content threshold for landslide predictions and early warning. The volume of water depends
217 on soil hydraulic properties, rainfall, initial moisture content, and domain geometry. The total volume
218 of water was more in Case 2 than in Case 1 because of the larger soil volume in Case 2 (56.44 m^3)
219 compared to Case 1 (48.88 m^3). The volume of water for both cases increased from 6th August 2018,

220 corresponding to the rainfall event on that day. On 9th August 2018, 253.6 mm/day rainfall was received
221 in this area. A sudden increase in volume of water in the domain was observed from 8th to 9th August
222 2018 for both cases (Fig. 6). Though the rainfall on 10th, 11th, and 12th August was less than the rainfall
223 on the 9th August, volume of water in soil did not show a considerable decrease. This indicates that the
224 volume of water added to soil due to the rainfall on 9th August 2018 was drained at a slow rate in the hill
225 slope. This was mainly because of lateritic soil in this region with clay and slit particles which retain
226 water in the pores for a long time even after rainfall stops (Easton & Bock, 2016). Moisture content in
227 soil reached its maximum on 16th August 2018 with 20.77 m³ of water in Case 1 and 23.98 m³ of water
228 in Case 2. On this day, the hillslope received the maximum rainfall (291.8 mm/day).



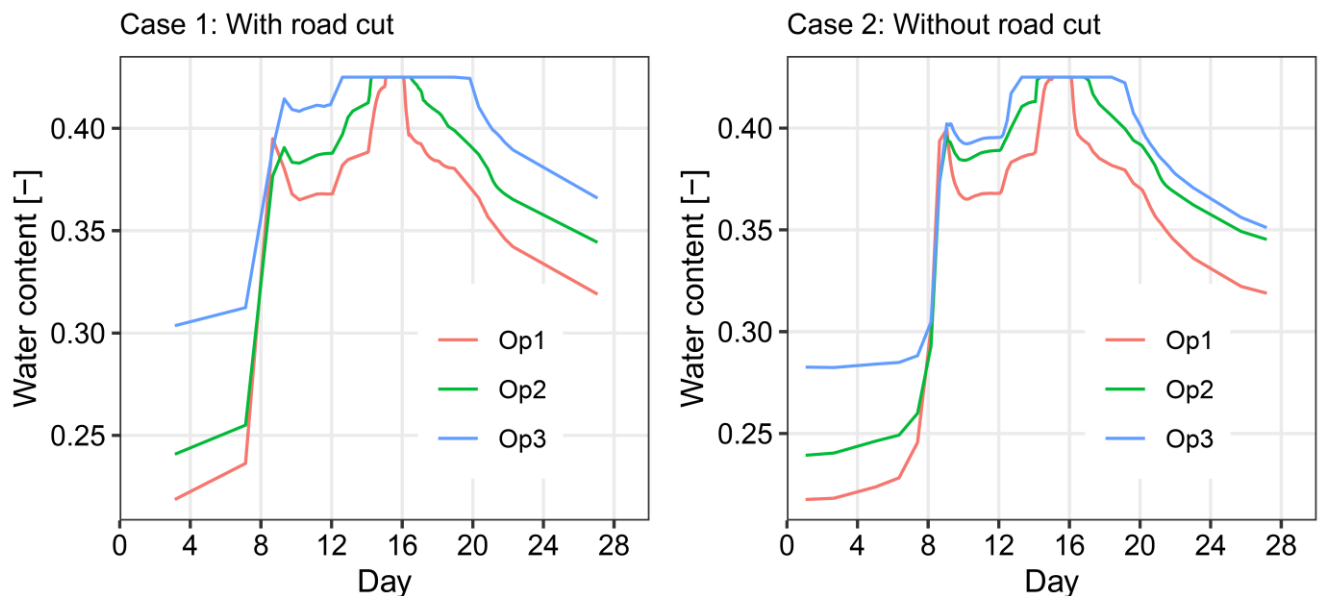
229

230 Fig. 6. The total volume of water in the domain for Case 1 (with road cut) and Case 2 (without road
231 cut).

232 3.2. Variation in the moisture content at observation points

233 Water content in the soil's pores leads to pore water pressure (PWP). Changes in water content at three
234 observation points (Op) (points 1, 2, 3 in Fig. 5) for Case 1 and Case 2 were analyzed. Water content
235 increased at all the Op's and reached a saturated condition (water content = 0.425) at different times.
236 The Op3 reached saturation earlier than the other two locations. This is because of the combined effect
237 of rainfall and the initial hydrostatic pressure head distribution assumed in the domain. Op2 reached the

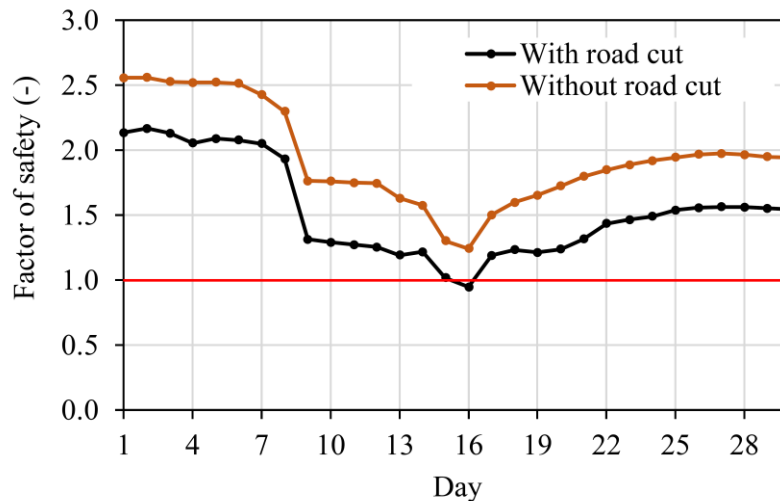
238 saturated condition earlier than Op1 for both cases. A maximum pressure head/water content is observed
 239 in the soil in all the observation points, approximately 15 to 16.5 days. Water content value equal to
 240 0.425 at any location and time corresponds to the saturated condition, and the water table will be at or
 241 above this point. Moisture variations at Op1 and Op2 were similar in both cases. The moisture content
 242 at Op3 in Case 1 reached the saturated condition earlier than Case 2. At Op3, Case 1 reached the saturated
 243 state in 12.15 days, and Case 2 reached the saturated condition in 13.5 days. It was also observed that
 244 moisture content remained in saturated condition for a longer time (from 12.15 to 19.85 days) at Op3 in
 245 Case 1 compared to Case 2 (which was from 13.50 to 18 days). The moisture content decreased slower
 246 (0.004/day after 20 days) for Case 1 compared to Case 2 (0.0084/day after 20 days). This shows that
 247 the specific hill slope geometry in Case 1 retained the moisture in the soil for more time with a low rate
 248 of its decrease compared to Case 2. Soil moisture status has a crucial role in landslide initiation since
 249 the increase in moisture content increases the pore water pressure and decreases the shear strength
 250 (Abraham et al., 2020; Marino et al., 2020).



251
 252 Fig. 7. Change in the water content in the soil at three observation points (Op1, Op2, Op3) in the
 253 domain for Case 1 and Case 2.

254 **3.3. The factor of safety in the hill slope**

255 The factor of safety (FoS) is a crucial indicator of slope stability and is defined as the ratio of the resisting
 256 force to the driving force along a failure surface. An FoS equal to or greater than one represents that the
 257 slope is stable, and a value less than one represents likely failure. The FoS of the hill slope corresponding
 258 to the pore water pressure distribution (determined using HYDRUS-2D/3D) in the soil in August 2018
 259 was simulated using the GeoStudio- Slope/W.



260

261 Fig. 8. The factor of safety of the slip surface for Case 1 (with road cut) and Case 2 (without road cut)

262 Figure 8 shows the minimum FoS of the slip surface each day in August 2018 for Case 1 (with road cut)

263 and Case 2 (without road cut). The slope was found to be stable in Case 2 compared to Case 1. For both

264 cases, the FoS showed a sudden decrease after 8th August 2018. This corresponds to the (a) increase in

265 rainfall on the same day, (b) increase in moisture content, and (c) increase in pore pressure in the soil. A

266 minimum FoS was observed on 16th August 2018 (0.946) for Case 1. This day corresponds with the day

267 with maximum rainfall (291.8 mm/day), the maximum volume of water (23.98 m³) in the domain, and

268 a longer saturated soil condition in the hill slope (as discussed in sections 3.1 and 3.2). It was on this day

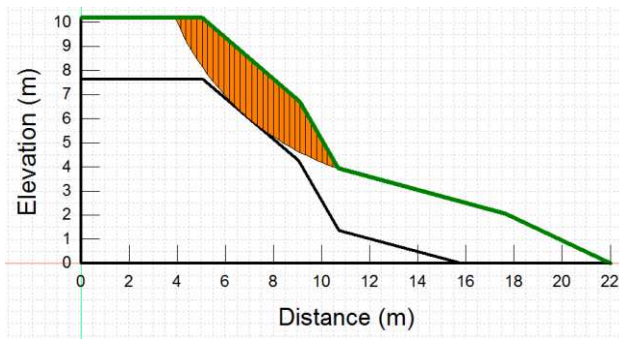
269 the actual landslide occurred in this location (a picture of the landslide is shown in Fig. 1). The weight

270 of the soil, geometry of the hill slope, and the moisture in the soil in Case 2 were such that the resisting

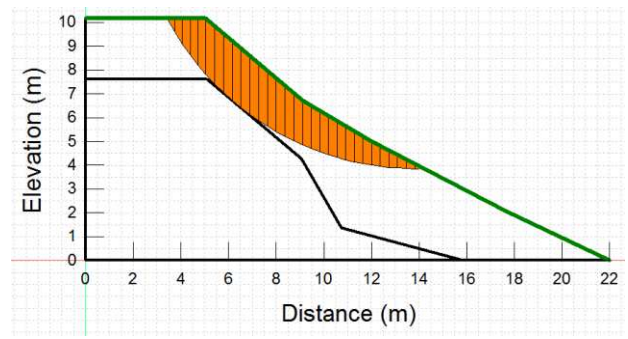
271 moment in the slide was greater than the activating moments, which resulted in FoS > 1. This shows that

272 the natural slope of the hill was able to prevent rainfall-induced landslides in the study area. Figure 9

273 shows the slip surface with minimum FoS for Case 1 (FoS= 0.946) and Case 2 (FoS= 1.243) on 16th
274 August 2018.



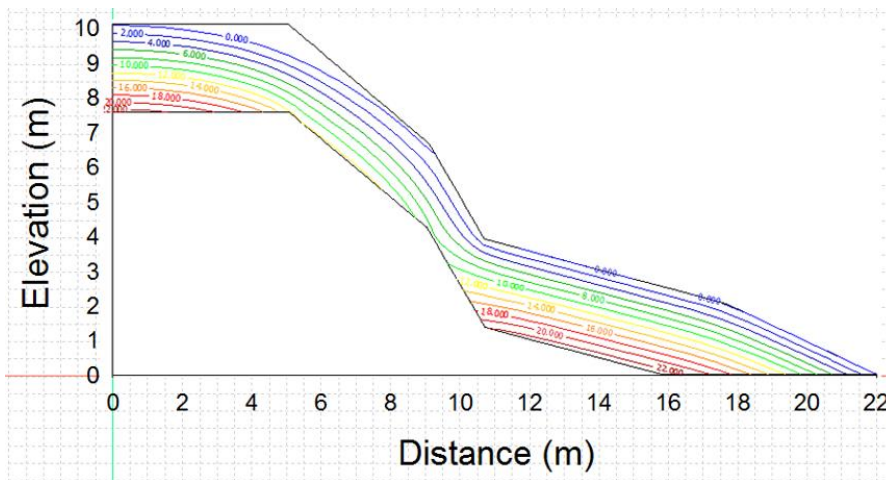
Case 1: With road cut



Case 2: Without road cut

275 Fig. 9. Slip surface with minimum Factor of Safety for Case 1 (with road cut) and Case 2 (without road
276 cut)

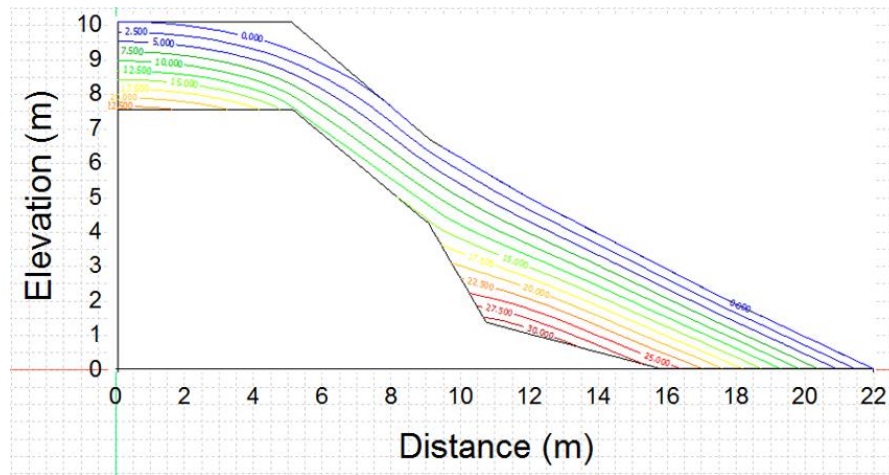
277 **3.4. Pore water pressure distribution**



278

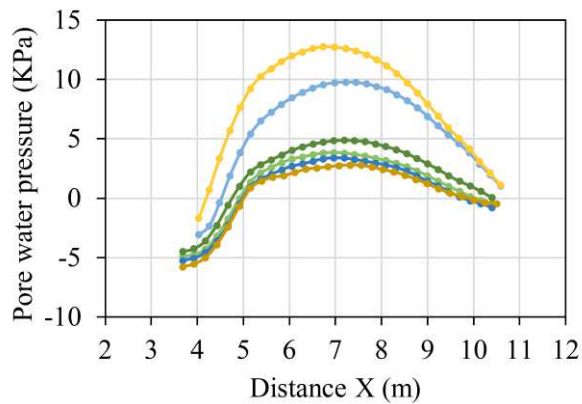
279

Case 1: With road cut

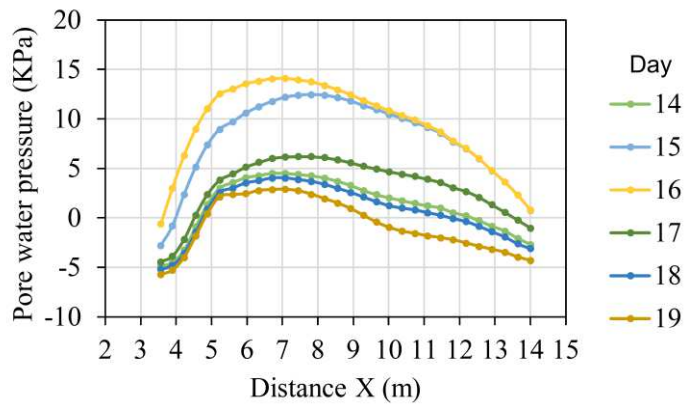


Case 2: Without road cut

Fig. 10. Pore water pressure distribution in the hill slope for Case 1 (with road cut) and Case 2 (without road cut) on 16th August.



Case 1: With road cut

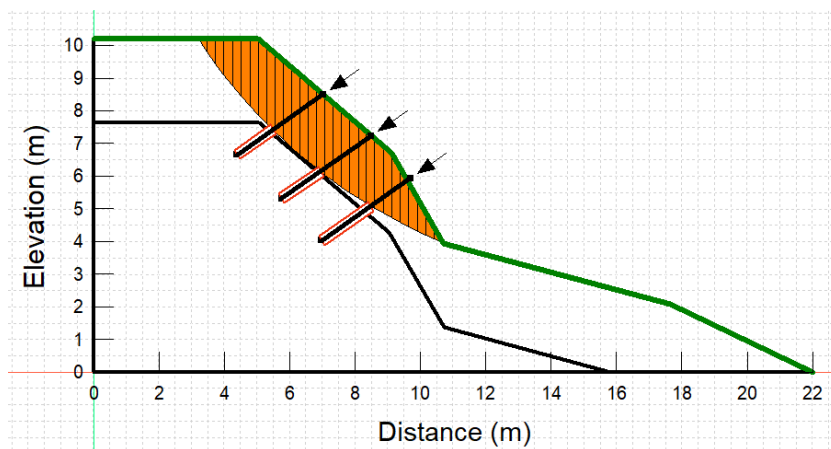


Case 2: without road cut

Fig. 11. Pore water pressure along the slip surface from 14th August 2018 to 19th August 2018 for Case 1 and 2.

Figure 10 shows the pore water pressure distribution in the soil for Case 1 and 2 on 16th August 2018 simulated using HYDRUS-2D/3D. The hill slope in Case 2 was subjected to larger pore water pressure than Case 1, with a maximum of 23 KPa and 31 KPa for Case 1 and 2, respectively. Figure 11 shows the pore water pressure along the slip surface from 14th August 2018 to 19th August 2018 for Case 1

293 and 2. For both cases, pore water pressure increased from 14th to its maximum at 16th and then decreased.
294 The pore water pressure is depended on the amount of saturation in the soil. Larger pore water pressure
295 was observed in Case 2 (14.5 KPa at a distance of 7 m) compared to Case 1(12.8 KPa at 6.8 m). It was
296 observed that Case 2 was more stable compared to Case 1 even when the pore water pressure along the
297 slip surface was more in Case 2. This shows that the geometry of the hill slope plays a predominant role
298 in keeping the slope stable. Glade, 2003; Jaboyedoff et al., 2016; Singh & Singh, 2013 also observed a
299 decreased hill slope stability with land-use change and artificial topographic interventions in hill slopes.



300
301 Fig. 12. Strengthening of the slope using nail reinforcement in Case 1 (hillslope with road cut). The
302 black arrow marks represent the location of the nail reinforcement.

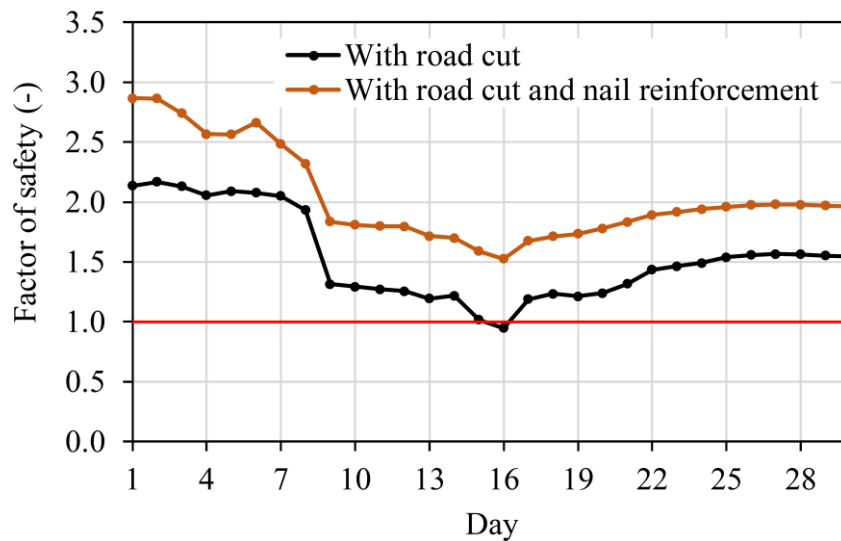
303
304 Several slope strengthening measures can be adopted to prevent the slope from failing (e.g., anchors and
305 piles, geosynthetic reinforcement, sheet pile walls, etc.). In this study, one of the strengthening measures
306 was studied to improve the slope stability in Case 1 (hillslope with road cut). Model simulations were
307 carried out to analyze the slope stability using a nail reinforcement (Fig. 12). This method of
308 reinforcement is generally used for strengthening the natural slope. Soil nails are included in GeoStudio-
309 SLOPE/W by defining the pull-out resistance, representing the amount of stress mobilized per unit area
310 at the interface between the nail and soil. Table 3 shows the nail specifications used in this case study.

311 Table 3. Specification of the nail reinforcement

Nail specifications	Value
The inclination of the nails	35°
Bond diameter: The diameter of the grouted section in contact with soil	0.3 m
Resistance reduction factor: This factor accounts for the nonlinear stress reduction over the embedded length	1.5
Pull-out resistance: This represents the amount of stress mobilized per unit area at the interface between the nail and soil	100 KPa
Tensile capacity	400 KN
Shear reduction factor: This accounts for the reduction of the tensile capacity due to physical processes such as installation damage, creep, and durability	1

312

313



314

315

316

Fig. 13. The factor of safety of the slip surface for Case 1 (with road cut) and the case with road cut and nail reinforcement.

317

318 Figure 13 shows the FoS of the slip surface in Case 1 (with road cut) and the case with road cut and nail
319 reinforcement corresponding to the rainfall in August 2018. It was observed that the FoS has improved
320 after incorporating the nail reinforcement throughout the month. The lowest FoS when there is no
321 reinforcement was observed as 0.946, and the lowest FoS after incorporation of the nail reinforcement
322 was found to be 1.524 on 16th August 2018. This demonstrates that strengthening measures can be
323 incorporated to improve the stability of this hillslope, and this can be analyzed using the integrated
324 modeling approach. A detailed investigation can be carried out to optimize the strengthening measure,
325 its design, and the related parameters.

326 **4. Conclusions**

327 In the context of a large number of landslides worldwide, it is essential to investigate the potential
328 solutions for its mitigation. This requires analysis of the landslide triggering mechanisms. Though
329 several triggering factors exist that independently and combinedly act upon a hill slope, the current study
330 focuses on slope stability analysis based on rainfall-induced pore water pressure in the soil, which is one
331 of the significant triggering mechanisms. A methodology for integrating existing models (HYDRUS-
332 2D/3D and GeoStudio- Slope/W) for simulating pore water pressure-induced landslides was developed.
333 As a case study to illustrate the methodology, a hill slope in Munnar, India, was investigated for its
334 stability corresponding to the ERE during August 2018. The stability analysis considered the pore water
335 pressure distribution in the soil corresponding to the daily variation in the rainfall in the hill slope. The
336 volume of water in the hill slope, temporal and spatial evolution of pore water pressure and factor of
337 safety were analyzed and correlated with the actual landslide that occurred in the study area. It was
338 observed that the slope was stable (with FoS equal to 1.243) when there was no road cut in the natural
339 slope of the hill, whereas the slope failed on 16th August 2018 in the case with road cut (with FoS equal
340 to 0.946). The integrated application of the simulation models (HYDRUS-2D/3D and GeoStudio-
341 Slope/W) effectively predicted the landslide that occurred in the study area on 16th August 2018. The

342 integrated model application also helped analyze the importance of the hill slope geometry in resisting
343 forces that drive the initiation of a slide. Though the pore water pressure was found to be more in Case
344 2 (without road cut) compared to Case 1 (with road cut), it was Case 1 that failed compared to Case 2.
345 A similar simulation modeling approach can be utilized for predicting landslides by anticipating extreme
346 rainfall conditions. The study also demonstrated the analysis of one of the strengthening measures (nail
347 reinforcement) for improving slope stability in Case 1 (hillslope with road cut) using the integrated
348 modeling approach.

349 **Software availability**

Simulation model: **HYDRUS-2D/3D**

Authors: M.Sejna and J.Simunek, Rien Van Genuchten

Copyright © 2006 - 2016:, PC-Progress s.r.o., Korunni 108a, Prague, Czech Republic

Contact details: hydrus@pc-progress.cz, admin@pc-progress.cz

Website: www.hydrus3D.com, www.pc-progress.com

Simulation model: **GeoStudio-Slope/W**

Developers: GEO-SLOPE International Ltd 1400, 633 – 6th Ave SW Calgary, Alberta, Canada T2P
2Y5

Contact details: info@geo-slope.com

Website: <http://www.geo-slope.com>

350

351 **References**

- 352 Abraham, M. T., Pothuraju, D., & Satyam, N. (2019). Rainfall thresholds for prediction of landslides
353 in Idukki, India: An empirical approach. *Water (Switzerland)*.
354 <https://doi.org/10.3390/w11102113>

355 Abraham, Satyam, N., Pradhan, B., & Alamri, A. (2020). Forecasting of Landslides Using Rainfall
356 Severity and Soil Wetness: A Probabilistic Approach for Darjeeling Himalayas. *Water*, *12*,
357 804. <https://doi.org/10.3390/w12030804>

358 Beegum, S., Šimůnek, J., Szymkiewicz, A., Sudheer, K. P., & Nambi, I. M. (2018). Updating the
359 Coupling Algorithm between HYDRUS and MODFLOW in the HYDRUS Package for
360 MODFLOW. *Vadose Zone Journal*, *17*(1).

361 Beegum, S., Šimůnek, J., Szymkiewicz, A., Sudheer, K. P., & Nambi, I. M. (2019). Implementation of
362 Solute Transport in the Vadose Zone into the “HYDRUS Package for MODFLOW.”
363 *Groundwater*, *57*(3), 392–408.

364 Brooks, R., & Corey, A. (1964). Hydraulic properties of porous media. *Hydrology Papers, Colorado*
365 *State University*, *3*(March), 37 pp. <https://doi.org/10.13031/2013.40684>

366 Bui, X.-N., Nguyen, H., Choi, Y., Nguyen-Thoi, T., Zhou, J., & Dou, J. (2020). Prediction of slope
367 failure in open-pit mines using a novel hybrid artificial intelligence model based on decision
368 tree and evolution algorithm. *Scientific Reports*, *10*(1), 9939. [https://doi.org/10.1038/s41598-](https://doi.org/10.1038/s41598-020-66904-y)
369 [020-66904-y](https://doi.org/10.1038/s41598-020-66904-y)

370 Carey, J. M., Massey, C. I., Lyndsell, B., & Petley, D. N. (2019). Displacement mechanisms of slow-
371 moving landslides in response to changes in porewater pressure and dynamic stress. *Earth*
372 *Surface Dynamics*, *7*(3), 707–722. <https://doi.org/10.5194/ESURF-7-707-2019>

373 Choudhury, D., Pain, A., & Rao, V. D. (2019). *Landslide investigations, kerala.*
374 *District Survey Report of Minor Minerals, Idukki district, Department of Mining and geology,*
375 www.dmg.kerala.gov.in. (2016).

376 Durner, W. (1994). Hydraulic Conductivity Estimation for Soils with Heterogeneous pore Structure. In
377 *Water Resources Research* (Vol. 30, Issue 2, p. 211;223). <https://doi.org/10.1029/93WR02676>

378 Easton, Z. M., & Bock, E. (2016). *Soil and soil water relationships*.

379 Fannin, R. J., & Jaakkola, J. (1999). Hydrological response of hillslope soils above a debris-slide
380 headscarp. *Canadian Geotechnical Journal*, 36(6), 1111–1122. <https://doi.org/10.1139/t99-074>

381 Fredlund, D. (1987). *Slope Stability Chapter 4 Slope Stability Analysis Incorporating the Effect of Soil*
382 *Suction*.

383 Fredlund, D. G., & Krahn, J. (1977). COMPARISON OF SLOPE STABILITY METHODS OF
384 ANALYSIS. *Canadian Geotechnical Journal*, 14(3), 429–439. <https://doi.org/10.1139/T77->
385 045

386 Geo-Slope. (2012). *Stability Modeling with SLOPE/W, an engineering methodology*.

387 Glade, T. (2003). Vulnerability assessment in landslide risk analysis. *Erde*, 134(2), 123–146.

388 Hopkins, T. C., Allen, D. L., & Deen, R. C. (1975). *Effects of Water on Slope Stability*. 44.

389 Huang, A. Bin, Lee, J. T., Ho, Y. Te, Chiu, Y. F., & Cheng, S. Y. (2012). Stability monitoring of
390 rainfall-induced deep landslides through pore pressure profile measurements. *Soils and*
391 *Foundations*, 52(4), 737–747. <https://doi.org/10.1016/J.SANDF.2012.07.013>

392 Jaboyedoff, M., Michoud, C., Derron, M.-H., Voumard, J., Leibundgut, G., Sudmeier-Rieux, K.,
393 Michoud, C., Nadim, F., & Leroi, E. (2016). Human-Induced Landslides: Toward the analysis
394 of anthropogenic changes of the slope environment. In *Landslides and Engineered Slopes.*
395 *Experience, Theory and Practice*. CRC Press.

396 Jalilzadeh, H., Hettiaratchi, J., Fleming, I., & Pokhrel, D. (2020). Effect of Soil Type and Vegetation
397 on the Performance of Evapotranspirative Landfill Biocovers: Field Investigations and Water
398 Balance Modeling. *Journal of Hazardous, Toxic, and Radioactive Waste*, 24.
399 [https://doi.org/10.1061/\(ASCE\)HZ.2153-5515.0000535](https://doi.org/10.1061/(ASCE)HZ.2153-5515.0000535)

400 Johnson, K. A., & Sitar, N. (1990). Hydrologic conditions leading to debris-flow initiation. *Canadian*
401 *Geotechnical Journal*, 27(6), 789–801. <https://doi.org/10.1139/t90-092>

402 Jones, S., Kasthurba, A. K., Bhagyanathan, A., & Binoy, B. V. (2021). Landslide susceptibility
403 investigation for Idukki district of Kerala using regression analysis and machine learning.

404 *Arabian Journal of Geosciences* 2021 14:10, 14(10), 1–17. <https://doi.org/10.1007/S12517->
405 021-07156-6

406 Kanda, E. K., Senzanje, A., & Mabhaudhi, T. (2021). Coupling Hydrus 2D/3D and AquaCrop Models
407 for Simulation of Water Use in Cowpea (*Vigna Unguiculata* (L.) Walp). In D. S.-K. Ting & A.
408 Vassel-Be-Hagh (Eds.), *Sustaining Tomorrow* (pp. 53–63). Springer International Publishing.
409 https://doi.org/10.1007/978-3-030-64715-5_4

410 Karandish, F., & Šimůnek, J. (2019). A comparison of the HYDRUS (2D/3D) and SALTMED models
411 to investigate the influence of various water-saving irrigation strategies on the maize water
412 footprint. *Agricultural Water Management*, 213, 809–820.
413 <https://doi.org/10.1016/j.agwat.2018.11.023>

414 Kim, J., Kim, Y., Jeong, S., & Hong, M. (2017). Rainfall-induced landslides by deficit field matric
415 suction in unsaturated soil slopes. *Environmental Earth Sciences* 2017 76:23, 76(23), 1–17.
416 <https://doi.org/10.1007/S12665-017-7127-2>

417 Klose, M., Damm, B., & Gerold, G. (2012). Analysis of Landslide Activity and Soil Moisture in
418 Hillslope Sediments Using Landslide Database and Soil Water Balance Model. *Geo-Öko*, 33,
419 204–231.

420 Kosugi, K. (1996). Lognormal Distribution Model for Unsaturated Soil Hydraulic Properties. *Water*
421 *Resources Research*, 32(9), 2697–2703. <https://doi.org/10.1029/96WR01776>

422 Kuriakose, S. L., Jetten, V. G., van Westen, C. J., Sankar, G., & van Beek, L. P. H. (2008). Pore water
423 pressure as a trigger of shallow landslides in the Western Ghats of Kerala, India: Some
424 preliminary observations from an experimental catchment. *Physical Geography*, 29(4), 374–
425 386. <https://doi.org/10.2747/0272-3646.29.4.374>

426 Lehmann, P., Gambazzi, F., Suski, B., Baron, L., Askarinejad, A., Springman, S. M., Holliger, K., &
427 Or, D. (2013). Evolution of soil wetting patterns preceding a hydrologically induced landslide
428 inferred from electrical resistivity survey and point measurements of volumetric water content

429 and pore water pressure. *Water Resources Research*, 49(12), 7992–8004.
430 <https://doi.org/10.1002/2013WR014560>

431 Liang, W. L. (2020). Dynamics of pore water pressure at the soil–bedrock interface recorded during a
432 rainfall-induced shallow landslide in a steep natural forested headwater catchment, Taiwan.
433 *Journal of Hydrology*, 587, 125003. <https://doi.org/10.1016/J.JHYDROL.2020.125003>

434 Marc, O., Stumpf, A., Malet, J.-P., Gosset, M., Uchida, T., & Chiang, S.-H. (2018). Towards a global
435 database of rainfall-induced landslide inventories: First insights from past and new events.
436 *Earth Surface Dynamics Discussions*, 1–28. <https://doi.org/10.5194/ESURF-2018-20>

437 Marino, P., Peres, D. J., Cancelliere, A., Greco, R., & Bogaard, T. A. (2020). Soil moisture
438 information can improve shallow landslide forecasting using the hydrometeorological threshold
439 approach. *Landslides*, 17(9), 2041–2054. <https://doi.org/10.1007/s10346-020-01420-8>

440 Matsuura, S., Asano, S., & Okamoto, T. (2008). Relationship between rain and/or meltwater, pore-
441 water pressure and displacement of a reactivated landslide. *Engineering Geology*, 101(1–2),
442 49–59. <https://doi.org/10.1016/J.ENGGEOL.2008.03.007>

443 Mishal, U., & Khayyun, T. (2018). *Stability Analysis of an Earth Dam Using GEO-SLOPE Model*
444 *Under Different Soil Conditions*. 36, 523–532. <https://doi.org/10.30684/etj.36.5A.8>

445 Morgenstern, N. R., & Price, V. E. (1965). The analysis of the stability of general slip surfaces.
446 *Geotechnique*, 15(1), 79–93. <https://doi.org/10.1680/GEOT.1965.15.1.79>

447 Oh, S., & Lu, N. (2015). Slope stability analysis under unsaturated conditions: Case studies of rainfall-
448 induced failure of cut slopes. *Engineering Geology*, 184, 96–103.
449 <https://doi.org/10.1016/j.enggeo.2014.11.007>

450 Petley, D. (2012). Global patterns of loss of life from landslides. *Geology*, 40(10), 927–930.
451 <https://doi.org/10.1130/G33217.1>

452 Rahardjo, H., Leong, E. C., & Rezaur, R. B. (2008a). Effect of antecedent rainfall on pore-water
453 pressure distribution characteristics in residual soil slopes under tropical rainfall. *Hydrological*
454 *Processes*, 22(4), 506–523. <https://doi.org/10.1002/HYP.6880>

455 Rahardjo, H., Leong, E. C., & Rezaur, R. B. (2008b). Effect of antecedent rainfall on pore-water
456 pressure distribution characteristics in residual soil slopes under tropical rainfall. *Hydrological*
457 *Processes*, 22(4), 506–523. <https://doi.org/10.1002/HYP.6880>

458 Rahimi, A., Rahardjo, H., & Leong, E. C. (2010). Effect of hydraulic properties of soil on rainfall-
459 induced slope failure. *Engineering Geology*, 114(3–4), 135–143.
460 <https://doi.org/10.1016/J.ENGGEOL.2010.04.010>

461 Schaap, M. G., Leij, F. J., Van Genuchten, M. T., & Brown, G. E. (2001). Rosetta: A computer
462 program for estimating soil hydraulic parameters with hierarchical pedotransfer functions.
463 *Journal of Hydrology*, 251, 163–176.

464 Simunek, J., Sejna, M., & van Genuchten, M. T. (2018). New features of version 3 of the HYDRUS
465 (2D/3D) computer software package. *JOURNAL OF HYDROLOGY AND*
466 *HYDROMECHANICS*, 66(2), 133–142. <https://doi.org/10.1515/johh-2017-0050>

467 Šimůnek, J., van Genuchten, M. Th., & Šejna, M. (2016). Recent Developments and Applications of
468 the HYDRUS Computer Software Packages. *Vadose Zone Journal*, 15(7), 0–0.
469 <https://doi.org/10.2136/vzj2016.04.0033>

470 Singh, C. D., & Singh, J. (2013). Landslides caused due to ignorance—Case studies from northeast
471 India. *Journal of the Geological Society of India*, 82(1), 91–94.

472 Spencer, E. (1967). A method of analysis of the stability of embankments assuming parallel inter-slice
473 forces. *Geotechnique*, 17(1), 11–26. <https://doi.org/10.1680/GEOT.1967.17.1.11>

474 Talebi, A., Uijlenhoet, R., & Troch, P. A. (2007). Soil moisture storage and hillslope stability. *Natural*
475 *Hazards and Earth System Sciences*, 7(5), 523–534. <https://doi.org/10.5194/nhess-7-523-2007>

- 476 Van Genuchten, M. T. (1980). A closed-form equation for predicting the hydraulic conductivity of
477 unsaturated soils 1. *Soil Science Society of America Journal*, 44(5), 892–898.
- 478 Vogel, T., & Cislerova, M. (1988). On the reliability of unsaturated hydraulic conductivity calculated
479 from the moisture retention curve. *Transport in Porous Media*, 3(1), 1–15.
480 <https://doi.org/10.1007/BF00222683>
- 481 Wasowski, J. (1998). Understanding rainfall-landslide relationships in man-modified environments: A
482 case-history from Caramanico Terme, Italy. *Environmental Geology*, 35(2), 197–209.
483 <https://doi.org/10.1007/s002540050306>
- 484 WHO. (2018). *United Nations Office for Disaster Risk Reduction (UNISDR) and the Centre for*
485 *Research on the Epidemiology of Disasters (CRED), part of the Institute of Health and Society*
486 *(Université catholique de Louvain)*.
- 487 Wicki, A., Lehmann, P., Hauck, C., Seneviratne, S. I., Waldner, P., & Stähli, M. (2020). Assessing the
488 potential of soil moisture measurements for regional landslide early warning. *Landslides*, 17(8),
489 1881–1896. <https://doi.org/10.1007/s10346-020-01400-y>
- 490 Xu, J., & Yang, X. (2018). Effects of Seismic Force and Pore Water Pressure on Three Dimensional
491 Slope Stability in Nonhomogeneous and Anisotropic Soil. *KSCCE Journal of Civil Engineering*,
492 22(5), 1720–1729. <https://doi.org/10.1007/s12205-017-1958-y>

493 **Statements and Declarations**

494 **Funding**

495 The authors declare that no funds, grants, or other support were received during the preparation of this
496 manuscript.

497 **Acknowledgments**

498 The authors would like to acknowledge the Kerala State Council for Science Technology and
499 Environment (KSCSTE) for involving them in the field investigation and analysis carried out by the

500 committee to examine the causes of repeated heavy rainfall events, subsequent floods, and landslides in
501 Kerala, 2020.

502 **Competing Interests**

503 The authors declare that there is no conflict of interest

504 **Author Contributions**

505 All authors contributed to the study's conception and design. Sahila Beegum, Jainet P J, Dawn Emil, K

506 P Sudheer, and Saurav Das performed material preparation, data collection, and analysis. Sahila

507 Beegum wrote the first draft of the manuscript. All authors commented on previous versions of the

508 manuscript. All authors read and approved the final manuscript.